EUROPHYSICS LETTERS 15 December 2005

Europhys. Lett., **72** (6), pp. 1011–1017 (2005)
DOI: 10.1209/epl/i2005-10332-7

Effects of resonant interminiband Zener tunneling on the terahertz frequency radiation in $GaAs/Al_{0.3}Ga_{0.7}As$ superlattices

PENG HAN, KUI-JUAN JIN(*), YUELIANG ZHOU, QING-LI ZHOU, HUI-BIN LU, DONG-YI GUAN and GUO-ZHEN YANG

Beijing National Laboratory for Condensed Matter Physics, Institute of Physics Chinese Academy of Sciences - Beijing 100080, PRC

received 25 July 2005; accepted in final form 19 October 2005
published online 11 November 2005

PACS. 73.21.Cd – Superlattices.
PACS. 73.40.-c – Electronic transport in interface structures.
PACS. 78.47.+p – Time-resolved optical spectroscopies and other ultrafast optical measurements in condensed matter.

Abstract. – The resonant interminiband Zener tunneling rate between two minibands in the process of terahertz (THz) radiation has been calculated with Kane model for two structures of $GaAs/Al_{0.3}Ga_{0.7}As$ superlattices with high electric field. From the theoretical results, it is found that Zener tunneling rate not only increases with the applied electric field F but also is very dependent on the width of the minibands and that of the gap between minibands. Without any fitting parameter, the calculated results agree well with the experimental data reported by Hirakawa and his co-workers. The results we obtained in this work demonstrate that the measured broadening in the spectra of terahertz emission and the observed oscillation in the intensity curve of terahertz emission in the high electric field region are indeed due to the resonant interminiband Zener tunneling. The good agreement with experimental results also indicates that Kane theory is good enough to model Zener tunneling rate when F is below 90 kV/cm in the system we worked on.

Terahertz (THz) radiation, having a frequency between microwave and laser, has a number of highly interesting applications in biological imaging, surface chemistry, and high-field condensed-matter studies [1]. There are many methods such as synchrotron radiation [2], two-dimensional plasmon in single quantum well excited by femtosecond laser pluses [3], and optical excitation at the thin-film surface [4] to generate THz radiation. Recently, THz emission was also observed from Bloch oscillations (BOs) in superlattices (SLs) [5] and super-SLs [6]. Because the tunneling into higher minibands is the main damping mechanism of BOs [7], the tunneling effect plays an important role in the THz emission.

Since Zener tunneling was first proposed in 1934 [8], considerable effort has been made to study this tunneling in multiple quantum wells transport [9], in spin polarization transport of ferromagnetic semiconductor [10], and in light wave tunneling of optical SLs [11]. Recently, it

(*) E-mail: kjjin@aphy.iphy.ac.cn

TABLE I – *The superlattices parameters and band structures for structures 1 and 2.*

Parameters	Structure 1	Structure 2
SLs Periods	73	55
Well width a (nm)	6.4	8.2
Barrier width b (nm)	0.56	0.8
First miniband (meV)	18–114	19–69
Second miniband (meV)	150–445	107–270
Band gap (meV)	36	38

was reported that the sudden broadening of THz emission spectra in the high field indicates the Zener tunneling into the higher miniband [12]. Furthermore, oscillations in the THz emission intensity in the high-field region reported in ref. [13] are also assumed due to the resonant interminiband Zener tunneling. Therefore, it is very important to clarify the effect of the interminiband Zener tunneling on the THz emission from the theoretical aspect.

In his famous paper [8], Zener first calculated the tunneling rate based on a semiclassical approach. Afterwards, Zener tunneling rate has been computed by perturbation theory on the basis of both Houston functions [14] and Kane [15] functions, leading to the same result [16]. However, the nonresonant tunneling, as described by the original Zener formula, and the resonant tunneling remains unclear. Recently, Glutsch [17] derived a formula for Zener tunneling rate in which both resonant and nonresonant Zener tunnelings have been taken into account. The improvement of this method is the application of different initial conditions. This method has been proved to be good enough by the optical absorption spectra experiment [17] when electric field F is below $60\,\mathrm{kV/cm}$ for the system Glutsch treated.

In this work, we calculated the interminiband resonant Zener tunneling rate in two structures of $GaAs/Al_{0.3}Ga_{0.7}As$ SLs under an electric field F using the method in ref. [16]. Many previous comparisons have been made for the calculated Zener tunneling rate with the line width of photon absorption corresponding to inter-band transition of electrons [18–20]. In this paper, we report the comparison for the calculated Zener tunneling rate with THz emission spectrum broadening [12] corresponding to electron transition between Wannier-Stark ladders (WSLs) in the conduction band. Very good agreement between our calculated Zener tunneling rates and the measured half-width at half-maximum (HWHM) of the THz spectra has been obtained. Furthermore, the F values at which peaks in the oscillation of the calculated Zener tunneling rate occur correspond to those at which peaks in the oscillation of the THz emission intensity occur in ref. [13]. These results give evidences that the broadening of spectra and the oscillations of the THz emission intensity in the high-field region are indeed due to the resonant interminiband Zener tunneling. In addition, the calculation method has been proved to be good enough to describe the Zener tunneling rate when F is below $90\,\mathrm{kV/cm}$ in our system.

The studied system is the undoped $GaAs/Al_{0.3}Ga_{0.7}As$ SLs. In our work the x-axis is regarded as the growth direction of the SLs; $d = a+b$ is the periodicity of the SLs, where a is the width of the well and b is the barrier width. In addition, $V(x) = V(x+ld)$ is the one-dimension lattice-periodic potential. Setting the zero reference energy at the bottom of GaAs conduction band edge, the barrier height is $250\,\mathrm{meV}$. To model these SLs of finite length, we regard ld as the positions of the centers of the wells with $l = 1, 2, \ldots, m$, where m is the total number of the SLs' periods. The energy bands of these two structures are calculated with Kronig-Penney model with a step size of $d/200$ and the Brillouin zone is sampled by 2000 points. The SLs parameters and the band structures for these two structures are summarized in table I.

The Hamiltonian H of an electron with charge $-e$ in the SLs under an applied field F in

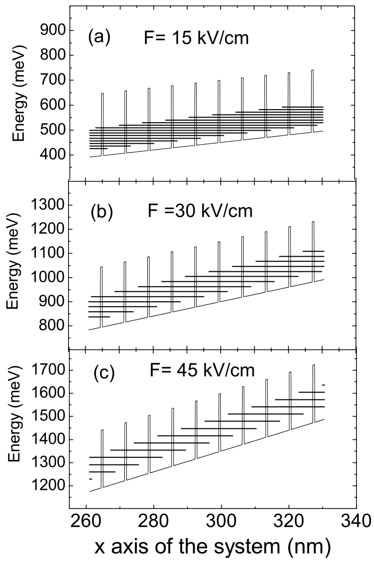

Fig. 1 – The band structures of structure 1 with various electric fields F.

the x-axis of the SLs is expressed as

$$H = -\frac{\hbar^2}{2\mu}\frac{\mathrm{d}^2}{\mathrm{d}x^2} + V(x) + eFx, \tag{1}$$

where, $\hbar$ is the reduced Planck constant and μ is the effective mass of the electron. From this Hamiltonian, the Zener tunneling rate has been derived by Glutsch [17]

$$\gamma = \frac{eFd}{2\pi\hbar}\int_{-\pi/d}^{+\pi/d}\mathrm{d}k_1\int_{-\pi/d}^{+\pi/d}\mathrm{d}k_2 f^*(k_1)g(k_1-k_2,B)f(k_2), \tag{2}$$

with

$$f(k) = X_{12}(k)\exp\left[\frac{1}{ieF}\int_0^k \mathrm{d}k'[E_1(k') + eFX_{11}(k') - E_2(k') - eFX_{22}(k')]\right], \tag{3}$$

and

$$g(k,B) = \sum_l \frac{\sin^2[(B-ld)\frac{\pi}{d}]}{[(B-ld)\frac{\pi}{d}]^2}e^{i(B-ld)k}; \quad B = \frac{\epsilon_{20}-\epsilon_{10}}{eF}, \tag{4}$$

where, k is the Bloch wave number. $E_n(k)$ (n is either 1 or 2) is the band energy without applied bias voltage, and ϵ is the eigenvalue of the Hamiltonian in eq. (1). The interminiband coupling parameter $X_{nn'}(k)$ is defined as $X_{nn'}(k) = \frac{i}{d}\int_{-d/2}^{+d/2}\mathrm{d}x u_{nk}^*(x)\frac{\mathrm{d}u_{n'k}(x)}{\mathrm{d}k}$, and $u_{nk}(x)$ is the period part of Bloch function.

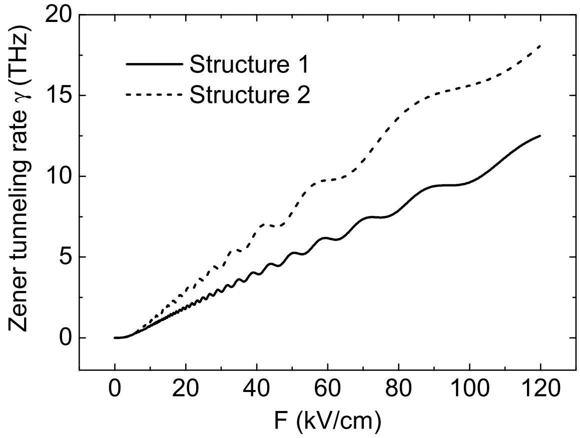

Fig. 2 – The theoretical Zener tunneling rate γ *vs.* electric field F.

The band structure of the SL under the influence of the electric field F has been plotted in fig. 1. It is shown that with the increasing of F, both the WSL energy separation eFd and the incline grade of the miniband increase.

Here, we use $\hbar\gamma$, which has the dimension of energy to describe the Zener tunneling rate. The calculated curves of $\hbar\gamma$ *vs.* F are plotted in fig. 2 for both those two structures. From this figure, it can be seen that Zener tunneling rates not only increase with the electric field F, but also exhibit pronounced oscillations due to the result of the interaction among WSLs [17] between two minibands. The function $g(k,B)$ in eq. (2) is the source of these oscillations with period $eFd/(\epsilon_{20}-\epsilon_{10})$. When F is not very large, $eFX_{nn'}(k)$ is much less than $E_n(k)$. Thus, ϵ_{10} and ϵ_{20} can be taken as the average energies of the first and second minibands, respectively. Therefore the structure with wider band width is with smaller period of the oscillation in the case that the miniband gaps are comparable for these two structures. Furthermore, we define $\epsilon_{20}-\epsilon_{10}$ as the average energy difference $\Delta\epsilon$. The values of $\Delta\epsilon$ for structures 1 and 2 are about 242 meV and 149 meV, and the periodicity d of SLs is 6.95 nm and 9.0 nm, respectively. Therefore, the ratio of oscillation period between these two structures is about 1 : 2, which can also be seen in fig. 2. Thus, the oscillation period of interminiband resonant tunneling rate is enhanced with the average energy difference of the minibands.

Because the second miniband of structure 1 is largely above the potential barrier, while that of structure 2 is slightly above the potential barrier, the wave function of the second miniband in structure 1 is much delocalized than that of the other. Furthermore, the average value of the miniband coupling parameter X_{12} for structures 1 and 2 is 4.563×10^{-4} cm and 6.323×10^{-4} cm, respectively. Thus, the coupling between two minibands of structure 1 is weaker than that of structure 2. In addition, the interminiband tunneling probability of structure 1 has been proved to be very small with Wentzel-Kramers-Brillouin (WKB) approximation, when the electric field strength is not too large [21]. Therefore, we can obtain that the structure with the second miniband of the SLs below the barrier has larger tunneling rate than the structure in which the second miniband is above the barrier.

Let us now make a comparison with recent experimental results [12, 13]. The Fourier spectra of the THz emission of structure 2 is shown in ref. [12]. The shape of THz spectra

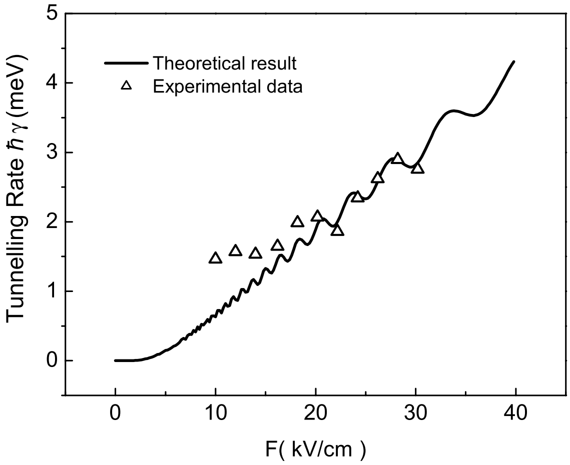

Fig. 3 – The tunneling rate, calculated using eq. (2), shown by the solid line and the experimental data obtained from ref. [12] shown by hollow triangles.

drastically changes and becomes very broad in the high-field region. The tunneling rate, which corresponds to the spectrum broadening, can be compared to the HWHM of the THz radiation spectra. The comparison between the theoretical results and the experimental data has been plotted in fig. 3. In the low-field region (between 10 kV/cm and 20 kV/cm), the dominant broadening mechanics is not Zener tunneling but the scattering of the randomly distributed Al atom in the barriers [22]. Thus, the calculated tunneling rate diverges from the measured spectrum broadening in this field region. In the high-field region (above 20 kV/cm), without any adjustable parameter, a good agreement between theoretical results and experimental data has been obtained. From this result, it can be found that the sudden broadening of the THz spectral shapes in the high field is indeed due to the resonant interminiband Zener tunneling. It should be noted that the experimental broadening includes the Zener tunneling broadening and the homogeneous broadening which is present also for $F = 0$, so the measured spectrum broadening is larger than the broadening caused only by Zener tunneling. On the other hand, the perturbation result from eq. (2) systematically overestimates the tunneling rate because of the $\pi/3$ problem [17]. Thus, both the experimental data and the theoretical result are a bit larger than the real Zener tunneling rate, which might be the reason why the agreement between them being so good in fig. 3.

Furthermore, the experimental THz emission intensity curves of structures 1 and 2 have been reported in ref. [13]. The samples 1 and 2 in that paper are corresponding to the structures 1 and 2 in this work, respectively. The experimental THz emission intensity curves are shown in figs. 4(a) and (c), and the calculated resonant interminiband Zener tunneling rates of these two structures are shown in figs. 4(b) and (d), respectively. In these figures, peaks of oscillations are marked with arrows. These marked numbers in the curves in figs. 4(b) and (d) correspond to the marked numbers in figs. 4(a) and (c). From these experimental data in figs. 4(a) and (c), it can be seen that with F larger than 40 kV/cm, the oscillations of THz emission intensity curves are observed on the tops of the broad peaks in the THz emission intensity curves. Comparing the theoretical results that we calculated with the experimental curves, it can be found that the F values at which peaks in the oscillation of the theoretical

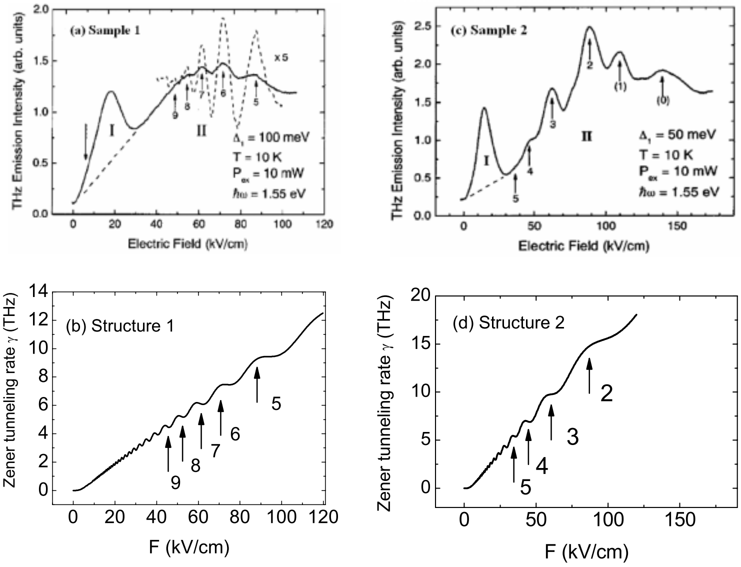

Fig. 4 – (a) and (c) are the experimental curves of THz emission intensity obtained from ref. [13]. (b) and (d) are the theoretical Zener tunneling rates of structures 1 and 2 *vs.* electric field F, respectively. The peaks of oscillations are marked with arrows denoted by the numbers corresponding to the experimental ones.

Zener tunneling rate occur correspond well to those at which peaks occur in the oscillation of the THz emission intensity when F is below $100\,\mathrm{kV/cm}$. We know that the wave functions in the SLs will be more localized with the increase of the electric filed F. Thus the overlap of wave functions between nearest WSLs will decrease, resulting in the decreasing of the THz emission intensity. On the other hand, the Zener tunneling between minibands becomes more important at high field, which cause the wave functions to be delocalized whenever the WSLs within two nearest minibands line up. Thus the THz emission intensity increases again. This competition of localization and delocalization of wave functions due to electric field and Zener coupling should be the reason for the oscillation in the observed THz emission intensity at high field.

We noticed that our calculated curve of structure 2 cannot explain the denoted peak 0 and peak 1 in the experimental curve of fig. 4(c). We think the reason is that these two peaks occur at larger electric field at which the perturbation theory is not valid anymore.

In summary, we have calculated the resonant interminiband Zener tunneling rate between two minibands by means of quantum-mechanical perturbation theory using the Kane functions as base functions. The tunneling rate increases with the electric field F, and shows pronounced oscillations as the result of interaction of WSLs between two minibands. The oscillation period of the interminiband resonant Zener tunneling rate increases with electric field and decreases with the miniband width of the superlattices. The excellent agreement between the theoretical HWHM and the experimental broadening of THz emission spectra [12] gives the evidence that the sudden brodening of THz spectra in high field is indeed due to Zener tunneling. We find that the competition of localization and delocalization of wave functions due to electric field and Zener coupling is the reason for the oscillation in the observed THz emission intensity at high field.

* * *

We gratefully acknowledge the financial support from the National Natural Science Foundation of China (No. 60321003). This work was also supported by the SIDA-Swedish Research Links (Grant No. 348-2002-6935).

REFERENCES

[1] ARNONE D. D., CIESLA C. M. and PEPPER M., *Phys. World*, **13** (2000) 35.
[2] NAKAZATO T., OYAMADA M., NIIMURA N. *et al.*, *Phys. Rev. Lett.*, **63** (1989) 1245.
[3] SEKINE N., YAMANAKA K., HIRAKAWA K. *et al.*, *Appl. Phys. Lett.*, **74** (1999) 1006.
[4] ASCAZUBI R., WILKE I., DENNISTON K., LU H. and SCHAFF W. J., *Appl. Phys. Lett.*, **84** (2004) 4810.
[5] WASCHK C., ROSKOS H. G. and SCHWEDLER R. *et al.*, *Phys. Rev. Lett.*, **70** (1993) 3319.
[6] SAVVIDIS P. G., KOLASA B., LEE G., and ALLEN S. J., *Phys. Rev. Lett.*, **92** (2004) 196802.
[7] LEO K., *High-Field Transport in Semiconductor Superlattices* (Springer-Verlag, Berlin Heidelberg) 2003.
[8] ZENER C., *Proc. R. Soc. London Ser. A*, **145** (1934) 523.
[9] CINELLI R. A. G., PIAZZA V., FRANCESCHI S. D. *et al.*, *Appl. Phys. Lett.*, **73** (1998) 3553.
[10] HALPERIN E. J., LOFGREEN D., KAWAKAMI R. K., YOUNG D. K., COLDREN L., GOSSARD A. C. and AWSCHALOM D. D., *Phys. Rev. B*, **65** (2002) 041306.
[11] GHULINYAN M., OTON C. J., GABURRO Z., PAVES L.I, TONINELLI C. and WIERSMA D. S., *Phys. Rev. Lett.*, **94** (2005) 127401 .
[12] SHIMADA Y., HIRAKAWA K., ODNOBLIOUDOV M. and CHAO K. A., *Phys. Rev. Lett.*, **90** (2003) 046806.
[13] SEKINE N., SHIMADA Y. and HIRAKAWA K., *Appl. Phys. Lett.*, **83** (2003) 4794.
[14] HOUSTON W. V., *Phys. Rev.*, **57** (1940) 194.
[15] KANE E. O., *J. Phys.Chem. Solids*, **12** (1959) 181.
[16] KRIEGER J. B. and IAFRATE G .J., *Phys. Rev. B*, **35** (1987) 9644.
[17] GLUTSCH S., *Phys. Rev. B*, **69** (2004) 235317.
[18] GLUTSCH S., BECHSTEDT F., ROSAM B. and LEO K., *Phys. Rev. B*, **63** (2001) 085307.
[19] GLÜCK M., KOLOVSKY A. R., KORSCH H. J. *et al.*, *Phys. Rev. B*, **65** (2002) 115302.
[20] ROSAM B., LEO K., GLÜCK M. *et al.*, *Phys. Rev. B*, **68** (2003) 125301 .
[21] JIN K.-J., ODNOBLYUDOV M., SHIMADA Y. *et al.*, *Phys. Rev. B*, **68** (2003) 153315.
[22] SEKINE N., SHIMADA Y. and HIRAKAWA K., *Appl. Phys. Lett.*, **83** (2003) 4794.